

Decoration of glass wool with zinc (II) phthalocyanine for the photocatalytic transformation of methyl orange

Azole Sindelo^a, Jonathan Britton^a, Anabel E. Lanterna^{b,c}, Juan C. Scaiano^b, Tebello Nyokong^{*a}

^a*Institute of Nanotechnology Innovation, Rhodes University, PO Box 94, Makhanda, 6140, South Africa.*

^b*Department of Chemistry and Biomolecular Science, Centre for Advanced Materials Research (CAMaR), University of Ottawa, 10 Marie Curie, Ottawa, ON K1N 6N5, Canada.*

^c*Current affiliation: School of Chemistry, University of Nottingham, University Park, NG7 2RD, UK*

Abstract

Zinc phthalocyanines containing one (mono carboxy phenoxy, ZnMCPc), four (tetra carboxy phenoxy, ZnTCPPc), and eight (tetra isophthalic acid, ZnTIPAPc) carboxyl groups were covalently conjugated to amine-functionalized glass wool (GW). The GW-Pcs were characterized and evaluated for singlet oxygen generation. The photocatalytic efficiencies of the GW-Pcs were assessed using methyl orange. Glass wool alone and the modified conjugates exhibited low to no photodegradation in the dark. The improved catalytic rate was observed for GW-ZnMCPc and GW-ZnTCPPc compared to GW-ZnTIPAPc due to the latter's lower singlet oxygen quantum yield generation. In addition, the modified glass wool was recyclable, making them suitable candidates for future environmental applications.

Keywords: Phthalocyanine, Glass wool, Methyl orange, singlet oxygen quantum yields, Photocatalysis

*Corresponding author. Tel: + 27 46 6038260, E-mail: t.nyokong@ru.ac.za. (T. Nyokong)

1. Introduction

Metallophthalocyanines (MPcs) are macrocyclic complexes with attractive qualities such as easy preparation in large quantities, structural modification, and thermal and chemical stability due to their π - conjugated structure [1]. These complexes have been used extensively in various applications. They are known to be one of the oldest dyes used in different areas of research, including catalysis, chemical sensors, liquid crystals, laser dyes, light-emitting diodes, nonlinear optics, photodynamic therapy (PDT), and photodynamic antimicrobial chemotherapy (PACT) [2-7]. Reactive oxygen species (ROS) such as singlet oxygen are essential for applications of Pcs as photocatalysts. MPcs containing heavy diamagnetic central metals have high singlet oxygen-generating abilities [8]; hence, this work focuses on using Zn as a central metal.

For practical applications in photocatalysis, immobilization of MPcs onto supports through either mixing, self-assembly, or covalent linkage [9-12] is important. Among these approaches, only covalent linkage can avoid catalyst leaching and contamination. Therefore, this work concentrates on chemically linking the MPcs to glass wool. Glass wool (GW) is an inexpensive, easily adaptable material commonly used for thermal insulation, filters, and adsorbent bed [13,14]. In this work, GW was modified with 3-aminopropyltriethoxysilane (APTES) [15] to provide amino groups for coordination to the COOH of the MPc. MPcs have been linked to supports such as electrospun fibers or membranes for the degradation of pollutants [16-18]; but, to the best of our knowledge, this is the first-time GW is linked to MPcs.

To test the photocatalytic activity of the GW-MPcs materials, methyl orange (an azo dye) is used as a model pollutant. Azo dyes are common synthetic dyes widely used in various

fields, including textile industries and paper printing, and is commonly found in industrial effluents [19]. Herein, we report on the photodegradation properties of a family of ZnPcs – mono carboxy phenoxy (ZnMCPPc), tetra carboxy phenoxy (ZnTCPPc), and tetra isophthalic acid (ZnTIPAPc) Zn phthalocyanines – when linked to GW to form GW-ZnMCPPc, GW-ZnTCPPc, and GW-ZnTIPAPc respectively.

2. Experimental

2.1. Materials

3-Aminopropyltriethoxysilane (APTES), tetrahydrofuran (THF), dimethylformamide (DMF), dimethyl sulfoxide (DMSO), *N,N'*-dicyclohexylcarbodiimide (DCC), anthracene-9,10-diyl-bis-methylmalonate (ADMA), ZnPc (standard), 1,3-diphenylisobenzofuran (DPBF), and methyl orange were purchased from Sigma-Aldrich. Deuterium oxide (D₂O) and ethanol were purchased from Merck. Non-treated glass wool Aldrich catalog #: 20384 was used. The syntheses of ZnMCPPc, ZnTCPPc, and ZnTIPAPc have been reported [20,21].

2.2. Synthesis

2.2.1. Glass wool functionalization (Scheme 1)

To three pretreated round bottom flasks (pretreatment is explained in the Supporting Information) containing 200 mL of high-performance liquid chromatography grade toluene were used to mix GW (1.00 g) and 2, 4, and 8 mL of APTES were added. The mixtures were refluxed at 110 °C for 18 h. The resulting APTES functionalized glass wools (GW-APTES) were vacuum filtered, washed with toluene and acetone, and dried in the oven

at 100 °C overnight. The resulting glass wools are represented as GW-2-APTES, GW-4-APTES, and GW-8-APTES, for 2, 4, or 8 mL APTES.

2.2.2. GW-Pc conjugate synthesis (Scheme 2)

GW-4-APTES (used for reasons explained below) was conjugated to ZnMCPc, ZnTCPPc, and ZnTIPAPc via an amide bond. The Pcs (ZnMCPc (5.7 mg, 0.008 mmol), ZnTCPPc (8.9 mg, 0.008 mmol) or ZnTIPAPc (10 mg, 0.008 mmol)) and DCC ((2.4 mg, 0.012 mmol), (9.7 mg, 0.048 mmol) and (19.4 mg, 0.096 mmol) for ZnMCPc, ZnTCPPc and ZnTIPAPc, respectively) were dispersed in dry DMF (5 mL) and stirred at room temperature for 24 h. After this time, the activated MPcs were separately added to three beakers containing GW-4-APTES (100 mg) immersed in dry DMF (10 mL). The mixtures were stirred at room temperature for 72 h. Then, the reaction mixtures were filtered under a vacuum, and the glass wool was washed with methanol, THF, water, and acetone; and dried in the oven. The glass wool was further purified on a Soxhlet extractor using water to remove any unbound MPcs producing blue GW-ZnMCPc, GW-ZnTCPPc, GW-ZnTIPAPc.

2.3. Photophysical and photochemical parameters

Fluorescence quantum yield for ZnMCPc, ZnTCPPc, and ZnTIPAPc was studied using the comparative methods previously reported [22] using ZnPc ($\Phi_F = 0.20$ [23]) in DMSO as a standard. The singlet oxygen quantum yield (Φ_Δ) for the Pcs in DMSO were determined using comparative methods with ZnPc as the standard in DMSO ($\Phi_\Delta = 0.67$ [24]) and DPBF as a quencher. Φ_Δ values for GW-ZnMCPc, GW-ZnTCPPc, and GW-ZnTIPAPc were studied using the absolute method reported before [25] using ADMA as a quencher (equations are shown in Supporting Information).

2.4. Photodegradation of methyl orange (MO)

GW-Pc (10 mg) conjugates were immersed in 3 mL of aqueous MO solutions ($1.65 - 8.25 \times 10^{-5}$ M) and illuminated with Modulight 690 nm laser (irradiance of 1.0 W/cm^2) at 15 min intervals. For reusability studies, the used glass wool was repeatedly washed with deionized water and air-dried overnight, and the process was repeated twice.

3. Result and Discussion

3.1. Characterization of Pc

Mono carboxy phenoxy (ZnMCPc), tetra carboxy phenoxy (ZnTCPPc), and tetra isophthalic acid (ZnTIPAPc) substituted zinc phthalocyanine was synthesized as reported in the literature [20,21] and they gave a satisfactory characterization data in this work, as reported in literature. The mass spectra (Fig. S1(A-C), Supporting Information) of ZnMCPc, ZnTCPPc, and ZnTIPAPc gave m/z peaks at 713.255 $[\text{M}]^+$, 1120.072 $[\text{M}]^+$, and 1299.655 $[\text{M}+4\text{H}]^+$, respectively, corresponding to the proposed zinc phthalocyanine structures. FT-IR spectra are also provided in the supporting information, Fig. S2. UV-Vis absorption spectra (in DMSO) for all complexes (Fig. 1A) show an intense single Q-band between 674-680 nm (Table 1), vibronic bands at 609-612 nm, and B-bands at 337-360 nm corresponding to reported values. The Q band redshifts with an increase in the number of COOH groups, even though it has been reported that MPc dyes containing 4, 8, or 16 carboxylic acid groups exhibited similar Q-band maxima [26]. Upon excitation at 610 nm, the MPcs exhibit weak fluorescence emission at 681-688 nm (Fig. 1B) with fluorescence quantum yields of 0.16, 0.09, and 0.06 for ZnMCPc, ZnTCPPc, and ZnTIPAPc, respectively. Thus, the fluorescence quantum yields decrease with the

increase in the number of COOH groups. The singlet oxygen quantum yield values for the complexes in DMSO ranged from 0.24 to 0.44.

3.2. Characterization of GW, GW-APTES, and GW-Pc conjugates

Commercial glass wool was functionalized with amine groups through the addition of APTES. The APTES treatment of the glass wool enabled the GW-Pc conjugation. The physical appearance of each sample is shown in Fig. 2. The attachment of APTES to GW (Scheme 1) was achieved through self-assembly, as reported in the literature [27].

3.2.1. Optimization

The amount of APTES attached to GW was evaluated by ^1H NMR spectroscopy (Figure S3). Using the quantitative NMR method (and maleic acid as a standard), duplicates of each sample (GW-2-APTES, GW-4-APTES, and GW-8-APTES) were tested as reported before [28]. GW-2-APTES showed no APTES content, meaning little or no APTES was attached to GW. For GW-4-APTES and GW-8-APTES, three individual signals (multiplets) at 2.35-2.42, 1.29, and 0.27-0.23 ppm corresponding to the CH_2 peak present on the APTES can be distinguished. Quantitative analysis of the APTES content suggests only GW-4-APTES has a measurable amount of APTES attached to the GW. Henceforth, only the results for GW-4-APTES (0.96 mg (2.8 WT%) of APTES in 34 mg of GW) will be discussed.

The amine moiety of the GW-4-APTES was reacted with the -COOH groups from the zinc phthalocyanine, forming an amide bond, Scheme 2. The linked conjugates were characterized using energy-dispersive X-ray (EDS), time-of-flight-secondary ion mass (ToF-SIMS), solid-state UV-Vis, and X-ray photoelectron spectroscopies and by scanning electron microscope (SEM).

3.2.2. Scanning electron microscope (SEM) and energy-dispersive X-ray spectroscopy (EDS)

Figure 3 shows SEM images of the unmodified and modified GWs. Pristine GW shows a glass fiber with small NaCl crystalline particles attached [15]. Upon modification, the GWs retain the same roughness and diameter of the glass fiber. The estimated elemental composition for GW, GW-APTES, ZnTIPAPc, and GW-ZnTIPAPc was determined by EDS and is shown in Fig. 4. EDS analysis shows that commercial glass wool contained various elements, including Na, Si, and Ca. Upon modification with APTES, there was evidence of N content and an increase in the intensity of Si, confirming the presence of APTES in the glass wool. The GW-ZnTIPAPc spectrum shows an increased intensity of N (when compared to APTES-GW) and a Zn peak, attributed to the conjugation of the zinc phthalocyanine.

3.2.3. Time-of-flight-secondary ion mass spectrometry (ToF-SIMS)

ToF-SIMS was used to study the mass distribution of GW, GW-APTES, and GW-ZnTCPPc, Fig. 5. The positive mode was used to assess the intensities of CH_3O^+ ($m/z = 31.03$) and C_3H_7^+ ($m/z = 43.09$), which are characteristic peaks for APTES [29], and the negative mode was used to identify CN^- ($m/z = 26.02$) used as a marker for ZnPc [30]. As demonstrated in Fig. 5, C_3H_7^+ ions were present in all samples and increased upon adding APTES and the ZnPc. CH_3O^+ ions had a higher intensity in GW-APTES and were well distributed on the glass wool, confirming the presence of APTES. The decrease in intensity (compared to GW-APTES) observed for both C_3H_7^+ and CH_3O^+ masses on GW-

ZnTCPPc is due to ZnTCPPc covering some $C_3H_7^+$ / CH_3O^+ rich regions. The CN^- ions increased (compared to GW-APTES) by three folds following conjugating to CN^- rich ZnTCPPc.

3.2.4. X-ray Photoelectron Spectroscopy (XPS)

XPS was used to analyze the chemical composition of the GW, GW-APTES, ZnMCPc, and GW-ZnMCPc. The deconvoluted C1s and N1s spectra are shown in Fig. 6. The C 1s of GW showed two signals at 282.7 and 283.9 eV corresponding to C-C and C-H bonds, respectively [31], while the N 1s depicted no signal complimenting the EDS results. The C 1s spectra of the GW-APTES showed an additional peak at 286.3 eV related to the C-N peak arising from the attachment of APTES to the glass wool [32]. The high-resolution N 1s spectrum for GW-APTES exhibited two peaks at 397.3 and 398.9, assigned to $-NH_2$ and NH_3^+ [33], respectively. Typical C 1s and N 1s spectra were obtained for a carbonyl-containing Pc, whereby three peaks at 283.3 (C-C), 285.2 (C=N), and 237.1(COOR) eV were obtained for C1s, and two peaks at 397.9 (C-N=C), and 399.4 (N-H) eV were observed for N 1s [34,35]. The high-resolution spectra were further used to prove the formation of an amide bond between the ZnPcs and GW-APTES. The deconvoluted N 1s spectrum for GW-ZnMCPc showed an additional peak at 400 eV, corresponding to the N-C=O bond.

3.2.5. Thermogravimetric Analysis (TGA)

Furthermore, the loading of the ZnPc complexes onto the glass wool was determined using the TGA method [36]. The TGA thermograms of GW-APTES (TGA profile for GW was similar to the GW-APTES; hence GW is not included in the plot), ZnMCPc, and

GW-ZnMCPc are shown in Fig. 7 in the range of 50-800 °C under a nitrogen atmosphere. The weight loss observed was 1.22 %, 4.22 %, and 83.45 % for GW-APTES, GW-ZnMCPc, and ZnMCPc, respectively, at 800°C. Using the GW thermogram curve as a reference, the decomposition profiles of ZnPc in GW-Pcs were used to determine the loading values. The obtained values are summarized in Table 1. GW-ZnMCPc and GW-ZnTCPPc had slightly higher values of 0.0365 and 0.0334 wt% Pc on GW, while GW-ZnTIPAPc had a lower value of 0.0184 wt%. The lower loading observed for GW-ZnTIPAPc may be due to **aggregation**.

3.2.6. Solid-state UV-Vis electronic absorption spectra

The solid-state UV-Vis spectra of all the samples are shown in Fig. 1C. GW-APTES showed a slight enhancement in absorbance compared to GW from 550 nm to 350 nm. After conjugation, the phthalocyanine profile is maintained for all conjugates. The spectra of the GW-Pc conjugates showed the characteristic phthalocyanine Q band and the broadening of the B band region. Noticeably, the Q-bands appear to broaden and red-shift (Table 1), a feature commonly found in the solid-state of Pcs [37]. The broad peaks are expected in solid-state due to aggregation [38], which is judged by the split in the Q band with the low energy band being due to the monomer and the high energy band due to the so-called H-aggregate. Aggregation is due to the π - π stacking interaction of the aromatic rings of Pcs. Table 1 lists the peaks for the monomer. GW-ZnTIPAPc showed a more prominent peak due to the aggregate relative to the monomer peak than the other two Pcs. Hence GW-ZnTIPAPc showed more aggregation.

3.2.7. Singlet oxygen quantum yield (Φ_{Δ})

The ability of the photoactive glass wool to generate phototoxic singlet oxygen is essential. The rate of singlet oxygen produced was studied in the presence of anthracene-9,10-diyl-bis-methylmalonate (ADMA). A time-dependent degradation of the absorbance of ADMA was monitored spectroscopically (Fig. 8, using GW-ZnMCPc as an example) and the results are summarized in Table 1. Control experiments were conducted in the dark and showed negligible change (Fig. 8: insert). Upon photoirradiation, there was evidence of $^1\text{O}_2$ demonstrated by the decrease in ADMA absorption with an increase in the photoirradiation times (Fig. 8). The calculated singlet oxygen quantum yields were 0.38, 0.35, and 0.22 for GW-ZnMCPc, GW-ZnTCPPc, and GW-ZnTIPAPc. The low Φ_{Δ} value for GW-ZnTIPAPc is due to the higher degree of aggregation discussed above. Both GW-ZnMCPc and GW-ZnTCPPc showed less aggregation than GW-ZnTIPAPc with GW-ZnMCPc having a high Φ_{Δ} due to improved loading onto the glass wool. The studies were repeated in the presence of NaN_3 , a singlet oxygen inhibitor, and the efficacy of the photocatalyst to produce singlet oxygen decreased (Fig. 8: insert), further supporting GW-Pc conjugate's ability to produce singlet oxygen. In addition, Fig. 8 exhibited no absorption from the 500-800 nm region, confirming no leaching of the Pc from the conjugates.

3.3. Photocatalytic activity study

The phthalocyanines conjugated to glass wool were applied for methyl orange bleaching. For accuracy, the photocatalytic experiments were done in triplicate per GW-Pc sample.

3.3.1. Adsorption in the dark

The MO adsorption onto GW support was determined in 15 min intervals, and the % of adsorption is shown in Fig. S4 (Supporting Information). Adsorption is determined from the decrease in the UV-Vis absorption profile of MO. At the beginning of the study, 0-15 min, there was a considerable amount of dye adsorbed by all three GW-Pc conjugates. After 15 min, the adsorption rate stabilized. Henceforth, the kinetics studies discussed below include a 15 min equilibrium period in the dark.

3.3.2. UV-vis absorption spectroscopy studies

The photobleaching of methyl orange was conducted using pristine GW as a control and the ZnPc conjugated glass wools at different concentrations. The studies were completed using an MO solution at pH 7.2. The UV-vis absorption spectrum of methyl orange (Fig. S5) shows two bands at 275 nm (band related to benzene rings) and 466 nm (band related to the chromophore N=N) [39-41]. Fig. 9 shows the change in the absorption spectra of MO in the presence of GW, GW-ZnMCPc, GW-ZnTCPPc, and GW-ZnTIPAPc at varying irradiation times. There was a rapid decrease of the 466 nm band – suggesting the azo bond's decomposition and the formation of an amine-containing compound [42], and a steady blue shift of the benzene ring absorption from 275 to ~255 nm. Thus, the changes in the spectra are attributed to a photochemically induced process rather than dye surface adsorption.

3.3.3. Kinetic study

The kinetic study of the photo-bleaching of MO at different initial concentrations (1.65×10^{-5} M, 3.30×10^{-5} M, 4.95×10^{-5} M, 6.60×10^{-5} M, and 8.25×10^{-5} M) was carried out in the presence of 20 mg of GW-ZnMCPc, GW-ZnTCPPc, and GW-ZnTIPAPc. The linear

kinetic plots indicate that the reactions follow pseudo-first-order kinetics, Fig.10(A). The initial rates increased with the increase of MO concentration for both GW-ZnMCPc and GW-ZnTCPPc, while for GW-ZnTIPAPc, the converse was observed in Table 2. The initial rates for GW-ZnMCPc and GW-ZnTCPPc are comparable, while GW-ZnTIPAPc has a lower rate due to low singlet oxygen quantum yields for the latter, Table 2. The k_{obs} values decreased with increased MO concentrations. This means that the photocatalytic activity of the employed photocatalysts decreases as the amount of MO increases. The GW-ZnTIPAPc conjugate had more than doubled the half-life of both GW-ZnMCPc and GW-ZnTCPPc, further supporting the efficiency of the latter conjugates in degrading the pollutant. The k_{obs} values (and % efficiencies) are highly dependent on the concentration of the analyte, however, Table 3 shows that the values in this work are comparable to those reported in literature and even better in some cases [43-46].

Furthermore, the degradation of methyl orange (3.3×10^{-5} M) by the GW-Pc conjugates was investigated under different light sources, namely, white light ($\lambda \sim 380-750$ nm), in the presence of a blue light ($\lambda \sim 450-495$ nm), Thorlabs M530L3 LED ($\lambda \sim 530$ nm), Thorlabs M730L3 LED ($\lambda \sim 730$ nm) and Modulight 7710-690 RHO laser system ($\lambda \sim 690$ nm). For comparison, each light source was adjusted to the irradiance of 110 mW/cm^2 and the change in MO concentration is presented in Fig.10(B). From the results, the order of degradation activity was white light > 690 nm > 730 nm > blue light > 530 nm. The lack of Pc absorption intensity at 530 nm resulted in a lower degradation activity, while the combination of all the wavelengths (white light) produced the maximum degradation activity. This observation was important to establish the potential practical applications of the GW-Pcs nanocomposite in the presence of solar radiations.

3.3.4. Catalyst reusability

The stability of the conjugated Pc is imperative for these applications. Therefore, the photodegradation process was repeated three times. Each experiment was carried out under the same conditions. After each experiment, the photocatalysts were washed, air-dried, and reused. The kinetics data are summarized in Tables S1 and S2. The degradation efficiency after the third cycle was above 80% for both GW-ZnMCPc and GW-ZnTCPPc but lowered to 62.2% for GW-ZnMCPc when using an MO concentration of 3.30×10^{-5} mol/L. The decrease in activity may be due to the permanent adsorption of the products onto the support.

Furthermore, the integrity of the reused glass wool conjugates was assessed via SEM and solid-state UV-vis. After the final catalytic cycle, the photocatalysts were washed, air-dried, and prepared for analysis. The SEM micrographs (Fig. S6 (a-b)) showed that the GW-Pcs conjugates retained their structural integrity; the solid-state UV-vis (Fig. S6 (c)) showed no significant change after three photodegradation cycles. Due to this stability, the GW-Pc composite could be used for sustainable methyl orange degradation. The photodegradation of methyl orange using Pc based catalysts has been reported to yield poly(catechol) and 2-amino-5(3-hydroxy-4-oxo-cyclohexa-2,5-dienylideneamino)-benzene sulphonic acid as degradation products [47], using direct injection into ion trap mass spectrometer fitted with an electrospray ionization (ESI-MS).

3.5. Mechanism

The excitation of the photocatalysts initiates the photodegradation process (Scheme 3) from the ground state (S_0) to the singlet excited state (S_1). Due to the presence of heavy atoms from zinc-containing photocatalysts, the excited photocatalysts undergo

intersystem crossing to the triplet state (T_1), where it interacts with molecular oxygen to produce singlet oxygen or other reactive oxygen species (ROS), which causes photobleaching of MO.

4. Conclusion

Commercially available glass wool was successfully modified with amine groups and was linked to zinc phthalocyanines. The resulting photocatalysts were characterized using various techniques, and singlet oxygen production was determined in aqueous media. GW-Pcs conjugates exhibited low adsorption of the pollutant. The degradation of methyl orange relies on the production of singlet oxygen. After three cycles, these photocatalysts were recyclable, and two of them maintained over 80% catalytic activity. These results indicate promising properties of the GW-Pcs conjugates, and the ability to degrade organic pollutants has excellent potential in critical environmental applications.

Acknowledgments

This work was supported by the Department of Science and Innovation (DSI) and National Research Foundation (NRF), through DSI/NRF South African Research Chairs Initiative for Professor of Medicinal Chemistry and Nanotechnology (UID 62620), Rhodes University, the Natural Sciences and Engineering Research Council of Canada and the Canada Research Chairs program. We thank IDRC (Canada) for the generous support that enabled the research collaboration among South Africa (UID 109677), Kenya, and Canada.

References

1. A. B. Sorokin, Phthalocyanine metal complexes in catalysis, *Chem. Rev.* 113 (2013) 8152-8191.
2. I. Okura, Photosensitization of porphyrins and phthalocyanines, Gordon and Breach Publishers, Berlin, 2001.
3. D. Wöhrle, O. Suvorova, R. Gerdes, O. Bartels, L. Lapok, N. Baziakina, S. Makarov, A. Slodek, Efficient oxidations and photooxidations with molecular oxygen using metal phthalocyanines as catalysts and photocatalysts, *J. Porphyrins Phthalocyanines* 8 (2004) 1020–1041.
4. P. Gregory, Steamrollers, sports cars and security: phthalocyanine progress through the ages, *J. Porphyrins Phthalocyanines* 3 (1999) 468-476.
5. J. Chen, Z. Chen, Y. Zheng, S. Zhou, J. Wang, N. Chen, J. Huang, F. Yan, and M. Huang, Substituted zinc phthalocyanine as an antimicrobial photosensitizer for periodontitis treatment, *J. Porphyrins Phthalocyanines* 15 (2011) 293-299.
6. M. Wainwright, Photodynamic antimicrobial chemotherapy (PACT), *J. Antimicrob. Chemother.* 42 (1998) 13-28.
7. M. Managa, M.A. Idowu, E. Antunes, T. Nyokong, Photophysical behavior and antimicrobial activity of dihydroxosilicon tris(diaquaplatinum)octacarboxyphthalocyanine, *Spectrochim. Acta. A. Mol. Biomol. Spectrosc.* 125 (2014) 147–153.
8. H. Shinohara, O. Tsaryova, G. Schnurpfeil, D. Wohrel, Differently substituted phthalocyanines: Comparison of calculated energy levels, singlet oxygen quantum yields, photo-oxidative stabilities, photocatalytic and catalytic activities, *J. Photochem. Photobiol A: Chem.* 184 (2006) 50–57.

9. M. C. DeRosa, R. J. Crutchley, Photosensitized singlet oxygen and its applications, *Coord. Chem. Rev.* 233 (2002) 351-371.
10. F. Ali, S. B. Khan, T. Kamal, Y. Anwar, K. A. Alamry, A. M. Asiri, Anti-bacterial chitosan/zinc phthalocyanine fibers supported metallic and bimetallic nanoparticles for the removal of organic pollutants, *Carbohydr. Polym.* 173 (2017) 676-689.
11. J. J. Armao, I. Nyrkova, G. Fuks, A. Osypenko, M. Maaloum, E. Moulin, R. Arenal, O. Gadat, A. Semenov, N. Giuseppone, Anisotropic self-assembly of supramolecular polymers and plasmonic nanoparticles at the liquid–liquid interface, *J. Am. Chem. Soc.* 139 (2017) 2345-2350.
12. X. Ding, B-H Han, Metallophthalocyanine-based conjugated microporous polymers as highly efficient photosensitizers for singlet oxygen generation, *Angew. Chem. Int. Ed.* 54 (2015) 6536-6539.
13. M. Thirukumaran, L.V. Kannan, I. Sankar, Study on mechanical properties of glass wool/epoxy reinforced composite, *Int. J. Comput. Aided Eng. Technol.* 10 (2018) 15–25.
14. F. Armetta, C. Defilippi, C. Giordano, E. Caponetti, L. Marciniak, D. Hreniak, M. L. Saladino, Influence of cerium content and heat treatment on Ce: YAG@ glass wool nanostructures, *J. Nanopart. Res.* 152 (2019) 1-9.
15. A. Elhage, B. Wang, N. Marina, M. L. Marin, M. Cruz, A. E. Lanterna, J. C. Scaiano, Glass wool: a novel support for heterogeneous catalysis, *Chem. Sci.* 9 (2018) 6844-6852.

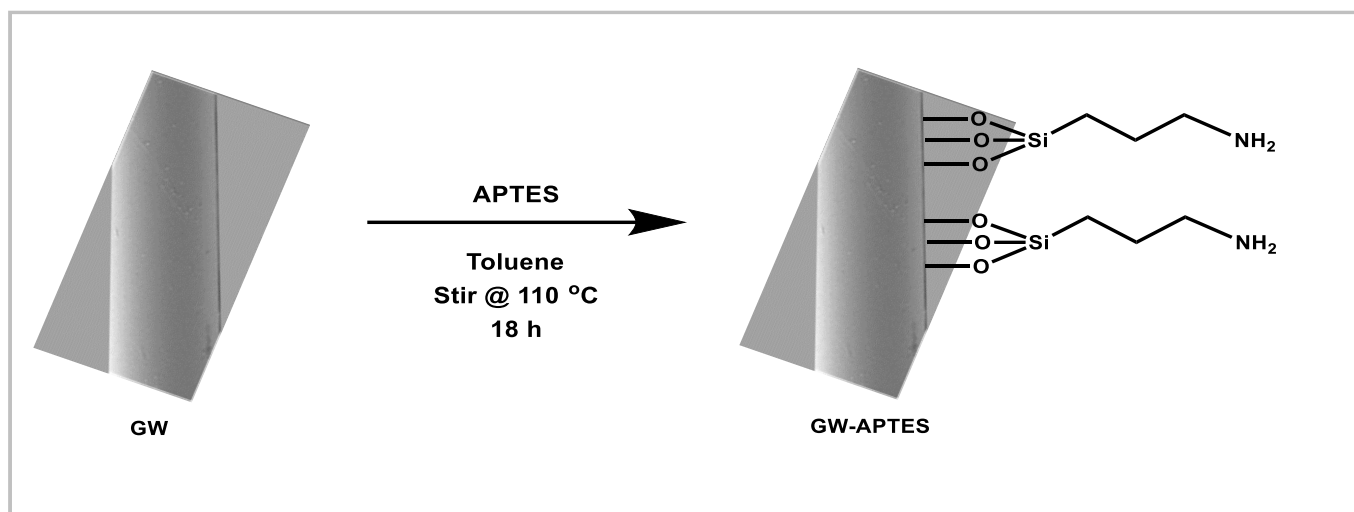
- 16.R. Zugle and T. Nyokong, Electrospun polyacrylic acid polymer fibers functionalized with metallophthalocyanines for photosensitizing and gas sensing applications, *J. Macro. Mol. Sci. A* 49 (2012) 279-287.
- 17.R. Zugle, C. Litwinski, N.Torto, T. Nyokong, Photophysical and photochemical behaviour of electrospun fibers of polyurethane polymer chemically linked to lutetium carboxyphenoxy phthalocyanine, *New J. Chem.* 35 (2011) 1588 – 1595.
- 18.D. M. Mafukidze, P. Mashazi, and T. Nyokong, Synthesis and characterization of polyacrylonitrile and polystyrene polymer conjugate assisted Pc anchored photoactive polymer asymmetric membranes, *Polym.* 105 (2016) 203-213.
- 19.B.C. Ventura-Camargo, M.A. Marin-Morales, Azo dyes: characterization and toxicity- a review, *textiles, Light Industrial Science and Technology (TLIST)* 2 (2013) 85-103.
- 20.Y. Li, T. M. Pritchett, J. Huang, M. Ke, P. Shao, W. Sun, Photophysics and nonlinear absorption of peripheral-substituted zinc phthalocyanine, *J. Phys. Chem. A* 112 (2008) 7200-7207.
- 21.M. Kimura, K. Nakada, Y. Yamaguchi, K. Hanabusa H. Shirai, N. Kobayashi, Dendritic metallophthalocyanines: synthesis and characterization of a zinc (II) phthalocyanine [8] 3-arborol, *Chem. Commun.* 13 (1997) 1215-1216.
- 22.S. Fery-Forgues, D. Lavabre, Are fluorescence quantum yields so tricky to measure? A demonstration using familiar stationery products, *J. Chem. Educ.* 76 (1999) 1260-1264.

23. A. Ogunsipe, J. Chen, T. Nyokong, Photophysical and photochemical studies of zinc (II) phthalocyanine derivatives—effects of substituents and solvents, *New J. Chem.* 28 (2004) 822-827.
24. N.A. Kuznetsova, N.S. Gretsova, V.M. Derkacheva, O.L. Kaliya, E.A. Lukyanets, Sulfonated phthalocyanines: aggregation and singlet oxygen quantum yield in aqueous solutions. *J. Porphyr. Phthalocyanines* 7 (2003) 147-154.
25. W. Spiller, H. Kliesch, D. Wöhrle, S. Hackbarth, B. Röder, G. Schnurpfeil, Singlet oxygen quantum yields of different photosensitizers in polar solvents and micellar solutions, *J. Porphyr. Phthalocyanines* 2 (1998) 145-158.
26. V. T. Verdree, S. Pakhomov, G. Su, M. W. Allen, A.C. Countryman, R.P. Hammer, S.A. Soper, Water Soluble Metallo-Phthalocyanines: The Role of the Functional Groups on the Spectral and Photophysical Properties, *J. Fluoresc.* 17 (2007) 547–563
27. H. H. Kyaw, S. H. Al-Harhi, A. Sellai, J. Dutta, Self-organization of gold nanoparticles on silanated surfaces, *Beilstein J. Nanotechnol.* 6 (2015) 2345-2353.
28. F. Kunc, V. Balhara, A. Brinkmann, Y. Sun, D. M. Leek, L. J. Johnston, Quantification and stability determination of surface amine groups on silica nanoparticles using solution NMR, *Anal. Chem.* 90 (2018) 13322-13330.
29. K. Awsiuk, A. Budkowski, A. Psarouli, P. Petrou, A. Bernasik, S. Kakabakos, J. Rysz, I. Raptis, Protein adsorption and covalent bonding to silicon nitride surfaces modified with organo-silanes: Comparison using AFM, angle-resolved XPS, and

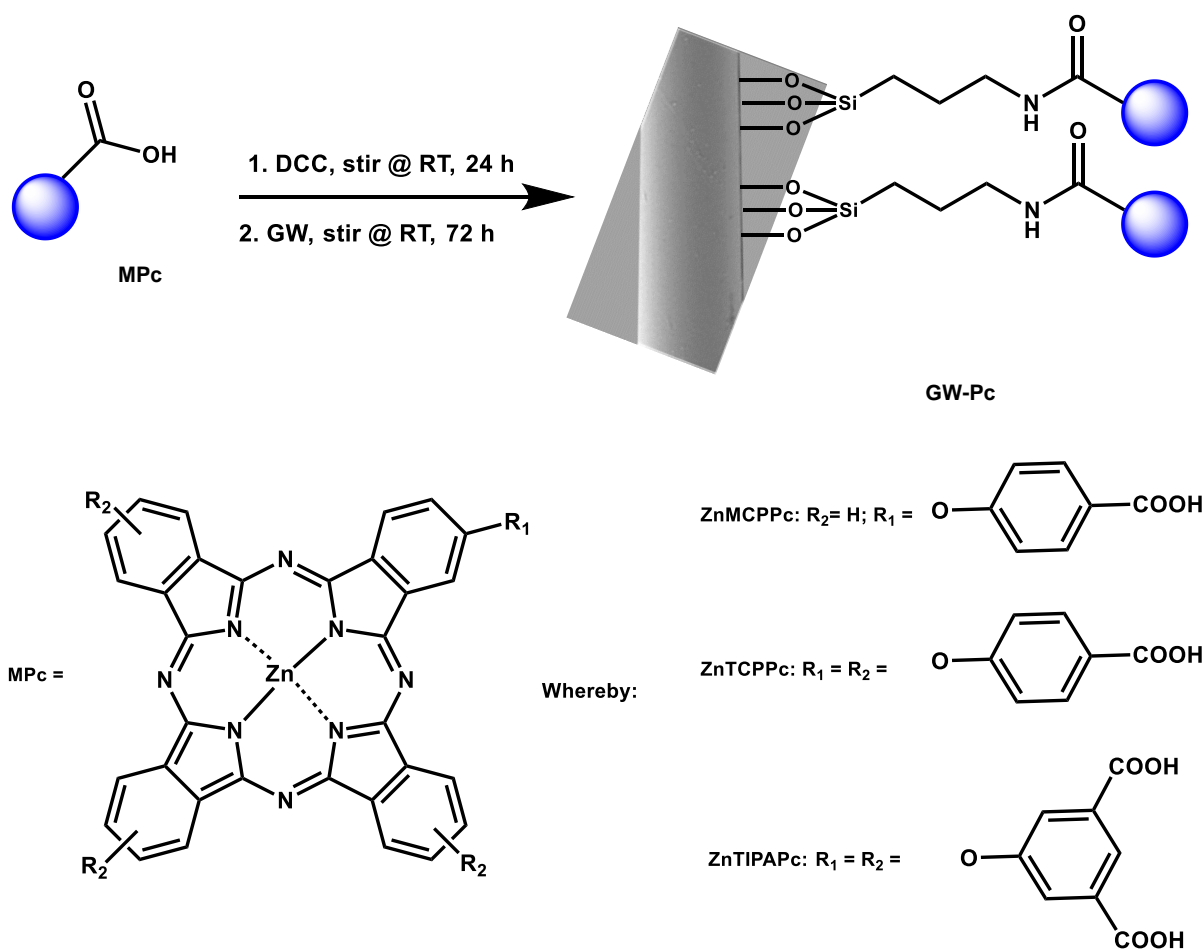
- multivariate ToF-SIMS analysis, *Colloids Surf. B Biointerfaces* 110 (2013) 217-224.
30. T. M. Kim, J. Whan Kim, H. S. Shim, J. J. Kim, High efficiency and high photostability zinc-phthalocyanine based planar heterojunction solar cells with a double interfacial layer, *Appl. Phys. Lett.* 101 (2012) 113301.
31. X. Chen, X. Wang, D. Fang, A review on C1s XPS-spectra for some kinds of carbon materials, *Fuller. Nanotub. Carbon Nanostruct.* 28 (2020) 1048-1058.
32. W. Sun, X. Lu, Y. Tong, J. Lei, G. Nie, C. Wang, A one-pot synthesis of a highly dispersed palladium/polypyrrole/polyacrylonitrile nanofiber membrane and its recyclable catalysis in hydrogen generation from ammonia borane, *J. Mater. Chem.* 2 (2014) 6740-6746.
33. H. Min, P. L. Girard-Lauriault, T. Gross, A. Lippitz, P. Dietrich, W. E. S. Unger, Ambient-ageing processes in amine self-assembled monolayers on microarray slides as studied by ToF-SIMS with principal component analysis, XPS, and NEXAFS spectroscopy, *Anal. Bioanal. Chem.* 403 (2012) 613–623.
34. O. Osifeko, T. Nyokong, Synthesis and physicochemical properties of zinc and indium phthalocyanines conjugated to quantum dots, gold, and magnetic nanoparticles, *Dyes Pigm.* 131 (2016) 186-200.
35. X. Ma, M. Luo, L. Yan, N. Tang, J. Li, Preparation of a magnetically recyclable visible-light-driven photocatalyst based on phthalocyanine and its visible light catalytic degradation of methyl orange and p-nitrophenol, *New J. Chem.* 43 (2019) 9589-9595.

36. K. Gulati, M. S. Aw, D. Losic, Nanoengineered drug-releasing Ti wires as an alternative for local delivery of chemotherapeutics in the brain, *Int. J. Nanomedicine* 7 (2012) 2069-2076.
37. A. Auger, P.M. Burnham, I. Chambrier, M.J. Cook, D.L. Hughes, X-Ray crystallographic studies of three substituted indium (iii) phthalocyanines: effect of ring substitution and the axial ligand on molecular geometry and packing, *J. Mat. Chem.* 15 (2005) 168-176.
38. L. Alagna, A. Capobianchi, M.P. Casaletto, G. Mattogno, M. Paoletti, G. Pennesi, G. Rossi, C. Nazionale, A.M. Paoletti, Effect of molecular packing on the solid-state spectra of ruthenium phthalocyanine: anomalous behaviour of a monodimensional stacked assembly, *J. Mater. Chem.* 11 (2001) 1928-1935.
39. E. Simonenko, A. Gomonov, N. Rolle, L. Molodkina, Modeling of H₂O₂ and UV oxidation of organic pollutants at wastewater post-treatment, *Procedia Eng.* 117 (2015) 337-344.
40. S. L. Chen, X. J. Haung, Z. K. Xu, Functionalization of cellulose nanofiber mats with phthalocyanine for decoloration of reactive dye wastewater, *Cellulose* 18 (2011) 1295-1303.
41. T. Shen, C. Jiang, C. Wang, J. Sun, X. Wang, X. Li, A TiO₂ modified abiotic–biotic process for the degradation of the azo dye methyl orange, *RSC Adv.* 5 (2015) 58704-58712.

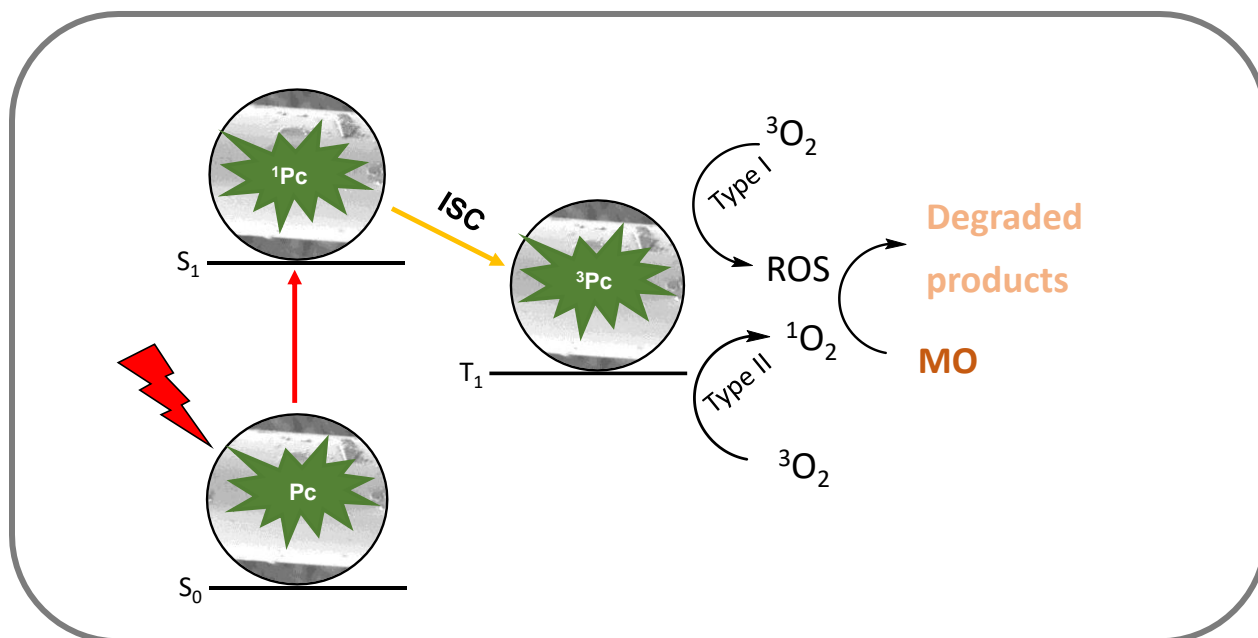
42. Y. Sha, I. Mathew, Q. Cui, M. Clay, F. Gao, X. J. Zhang, Z. Gu, Rapid degradation of azo dye methyl orange using hollow cobalt nanoparticles, *Chemosphere* 144 (2016) 1530-1535.
43. S. Mapukata, T. Nyokong, Development of phthalocyanine functionalised TiO₂ and ZnO nanofibers for photodegradation of methyl orange, *New J. Chem.* 44 (2020) 16340-16350.
44. L. Shao, H. Xie, J. Mo, Z. Yang, Z. Fan, C. Qi, Preparation of a novel nanofibrous mat-supported Fe (III) porphyrin/TiO₂ photocatalyst and its application in photodegradation of azo-dyes, *Environ. Eng. Sci.* 29 (2012) 807-813.
45. P. Khoza, T. Nyokong, Photocatalytic behavior of phthalocyanine-silver nanoparticle conjugates supported on polystyrene fibers, *J Mol Catal A Chem.* 395 (2014) 34-41.
46. Y. Yilmaz, Preparation of a Phthalocyanine-Nanometal-Coated Silica Microparticle Conjugate as Heterogeneous Photocatalyst and Investigation of Its Photocatalytic Activity, *Chemistry Select* 6 (2021) 7223-7231.
47. R. Zugle, T. Nyokong, Zinc(II) 2,9,16,23-tetrakis[4-(N-methylpyridyloxy)] phthalocyanine anchored on an electrospun polysulfone polymer fiber: Application for photosensitized conversion of methyl orange, *J. Mol. Catal. A: Chem.* 366 (2013) 247-253.



Scheme 1: Synthetic route illustrating the functionalization of glass wool with APTES.



Scheme 2: Conjugation of glass wool to phthalocyanine through amide bond formation.



Scheme 3: Mechanism for the formation of singlet oxygen and ROS species towards the photodegradation of methyl orange.

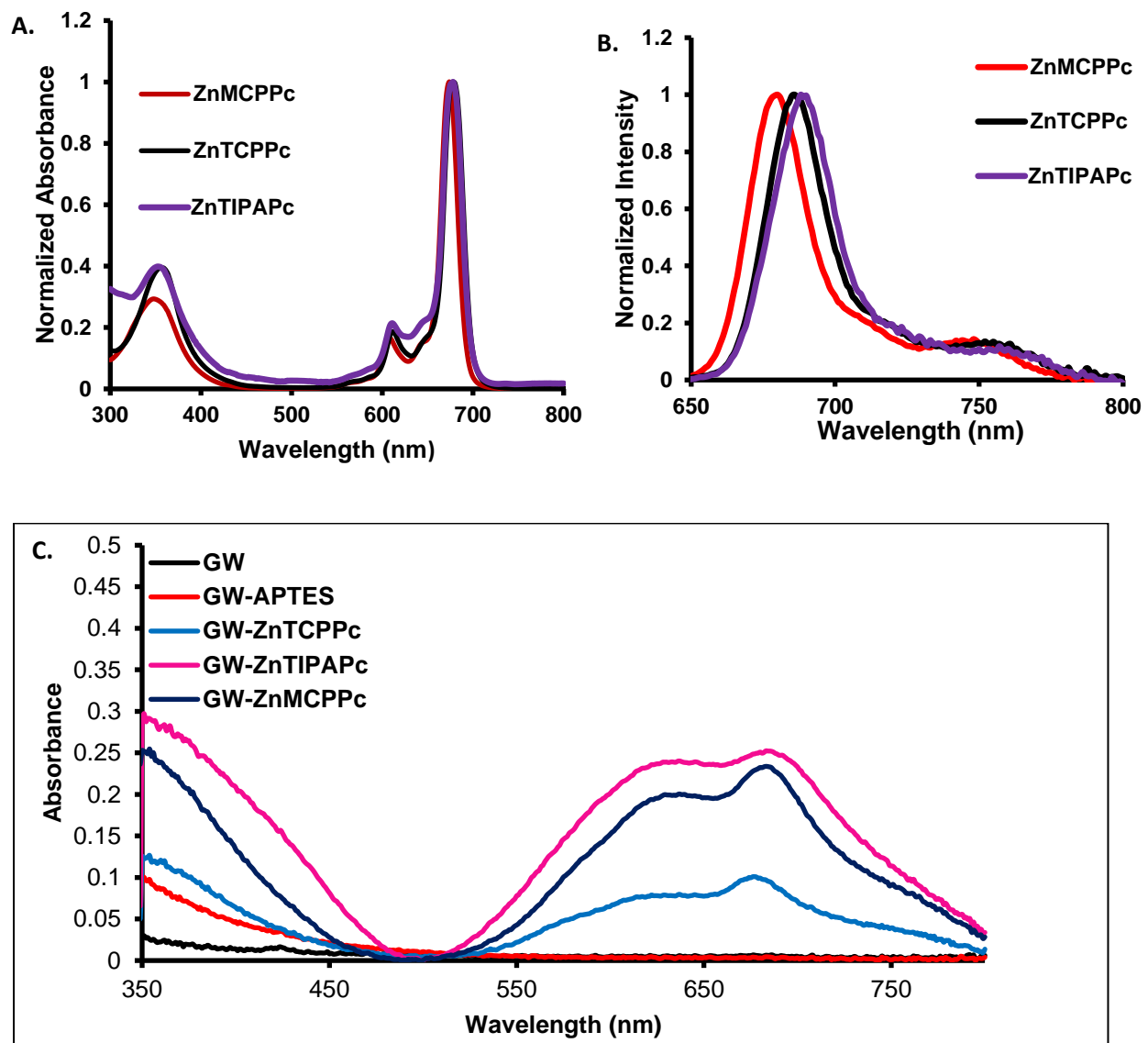


Figure 1: (A) Normalized UV-vis spectra and (B) emission spectra of ZnMCPc, ZnTCPPc, and ZnTIPAPc in DMSO. (C) Solid-state UV-Vis spectra of GW, GW-4-APTES, GW-ZnTCPPc, GW-ZnTIPAPc, and GW-ZnMCPc.

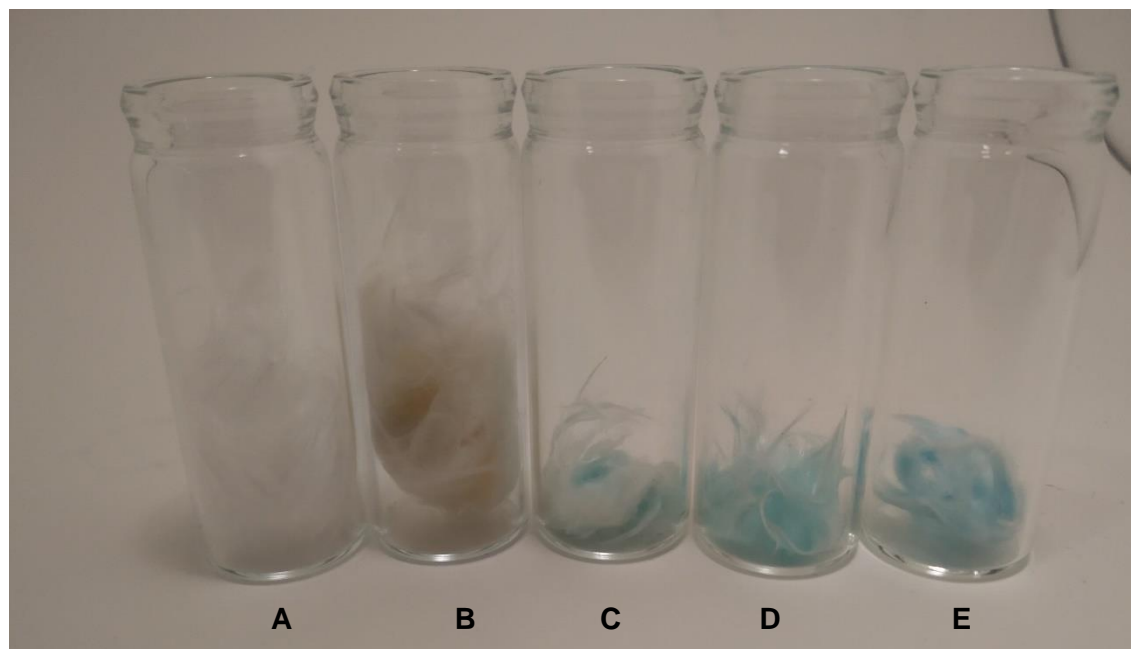


Figure 2: Glass wool images of (A) GW, (B) GW-APTES, (C) GW-ZnMCPPc, (D) GW-ZnTCPPc, and (E) GW-ZnTIPAPc.

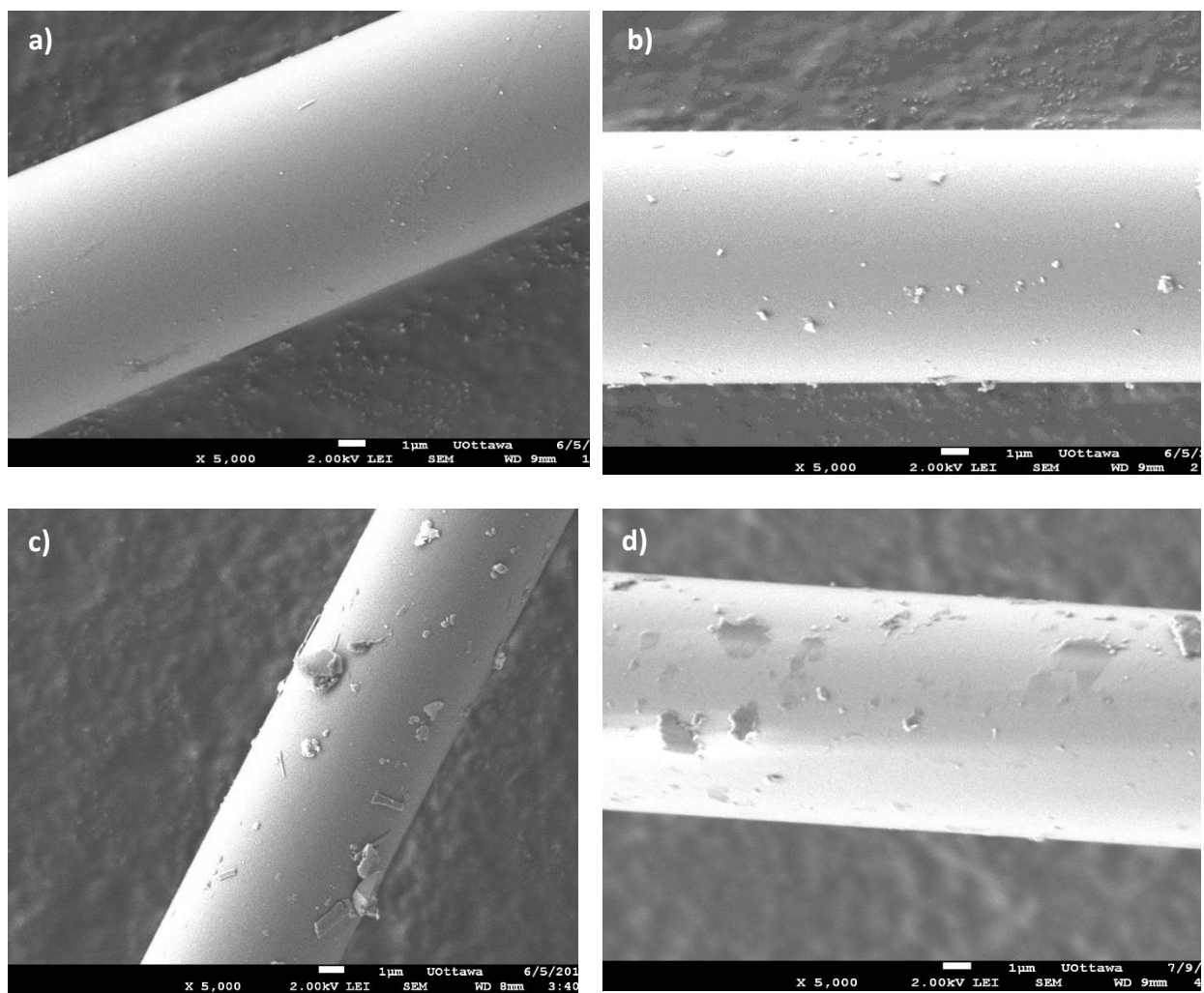


Figure 3: SEM micrographs for a) GW, b) GW-4-APTES, c) GW-ZnMCPPc, and d) GW-ZnTCPPc.

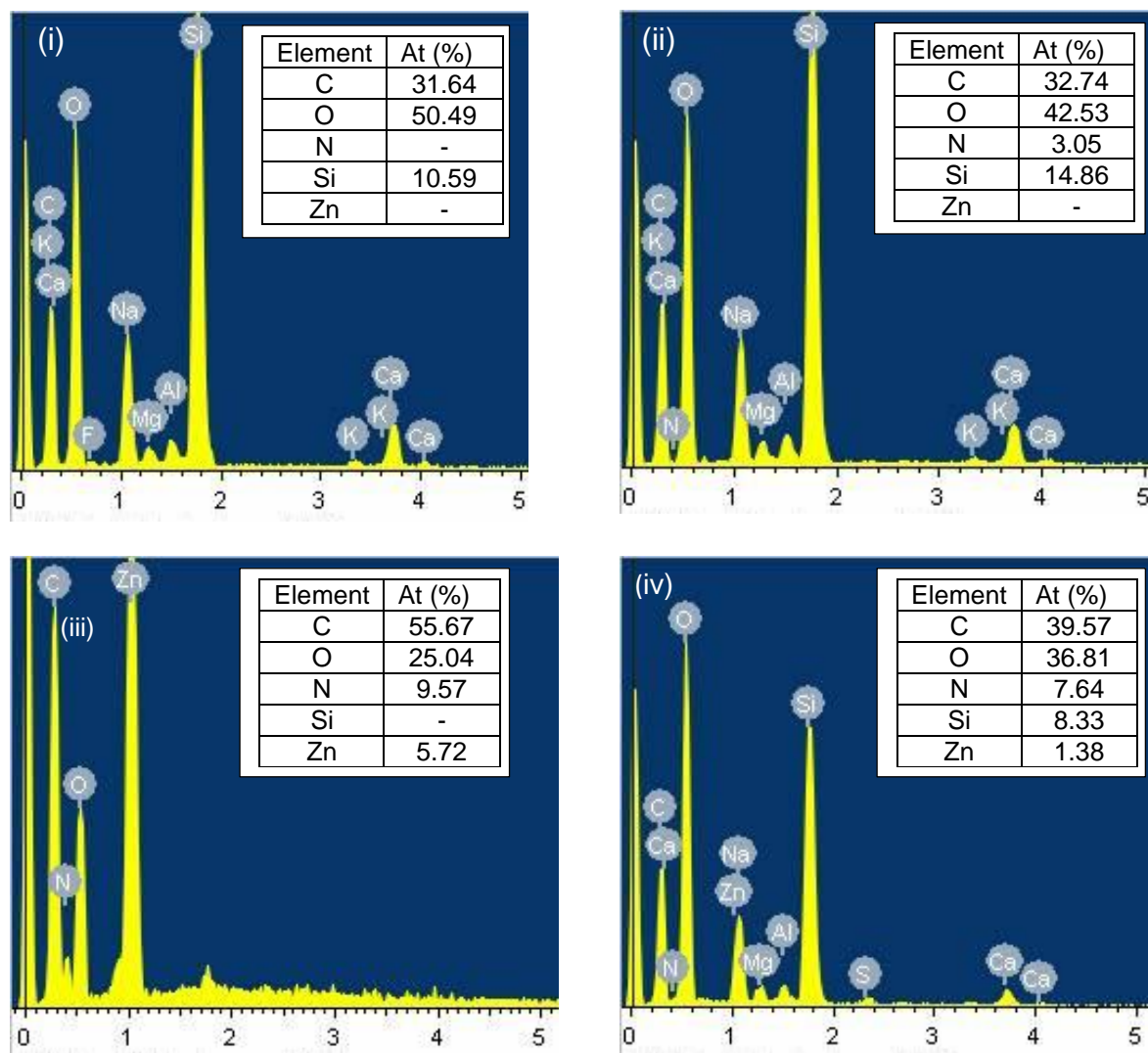


Figure 4: EDS spectra of (i) GW, (ii) GW-4-APTES, (iii) ZnTIPAPc, and (iv) GW-ZnTIPAPc.

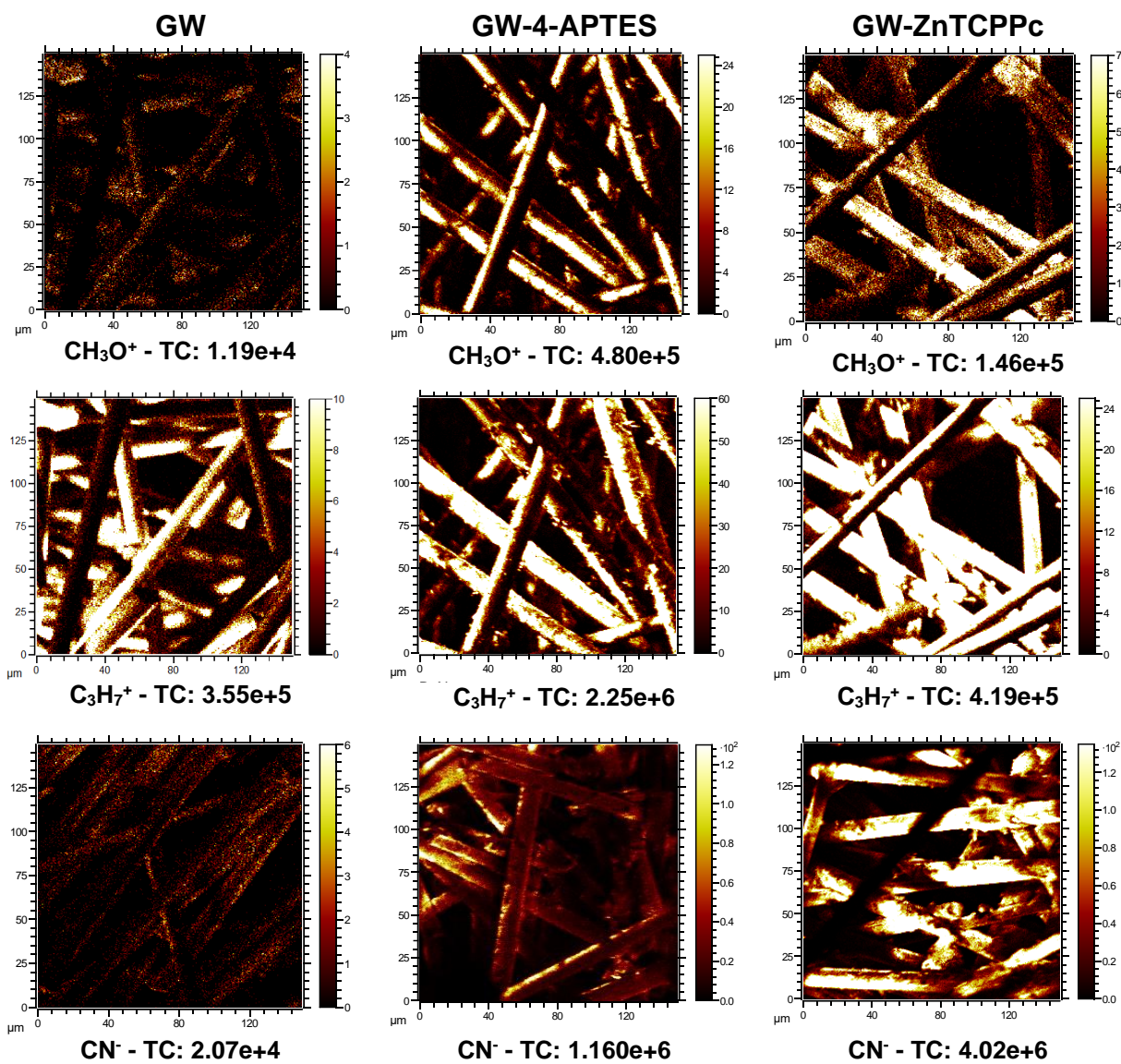


Figure 5: ToF-SIMS images of GW, GW-4-APTES, and GW-ZnTCPPc. The image area was $150 \mu\text{m} \times 150 \mu\text{m}$, and the total ion dose was $\sim 1.79 \times 10^{13}$ ions/cm².

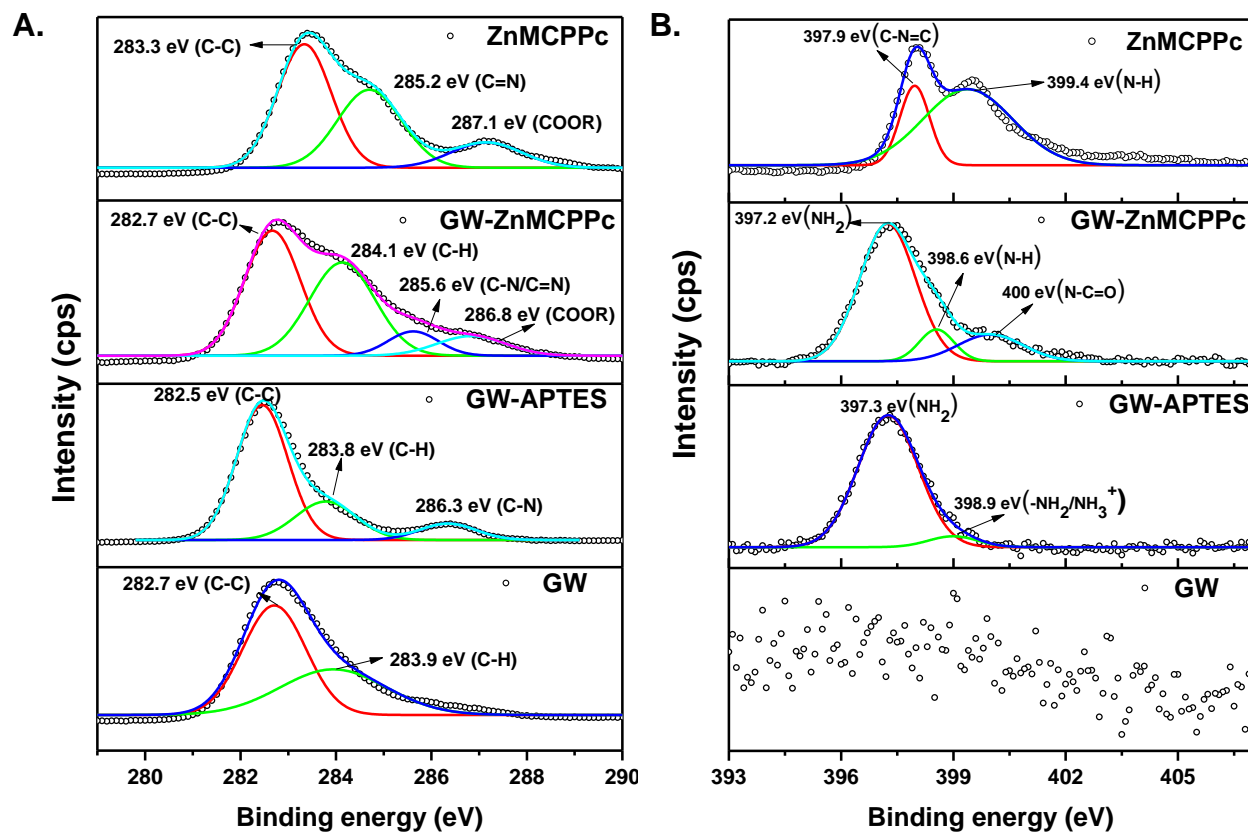


Figure 6: The deconvoluted (A.) C1s and (B.) N1s XPS spectra of GW, GW-APTES, GW-ZnMCPpC, and ZnMCPpC.

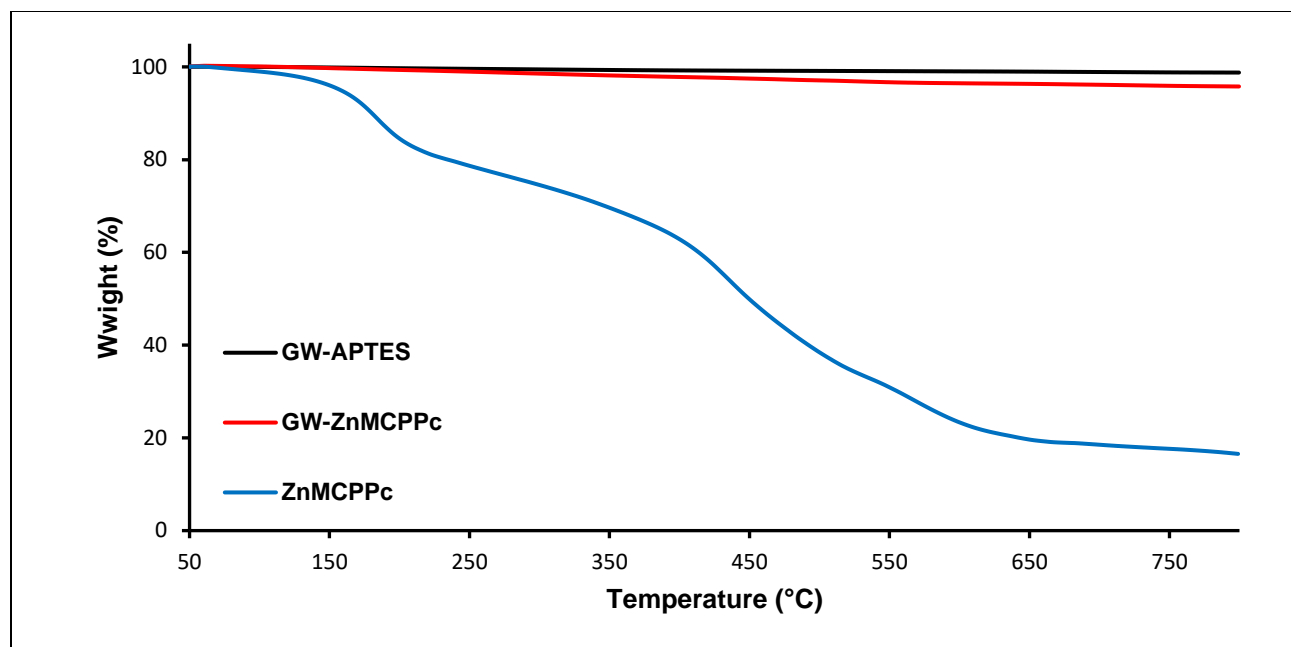


Figure 7: TGA thermograms of GW-APTES, GW-ZnMCPc, and ZnMCPc.

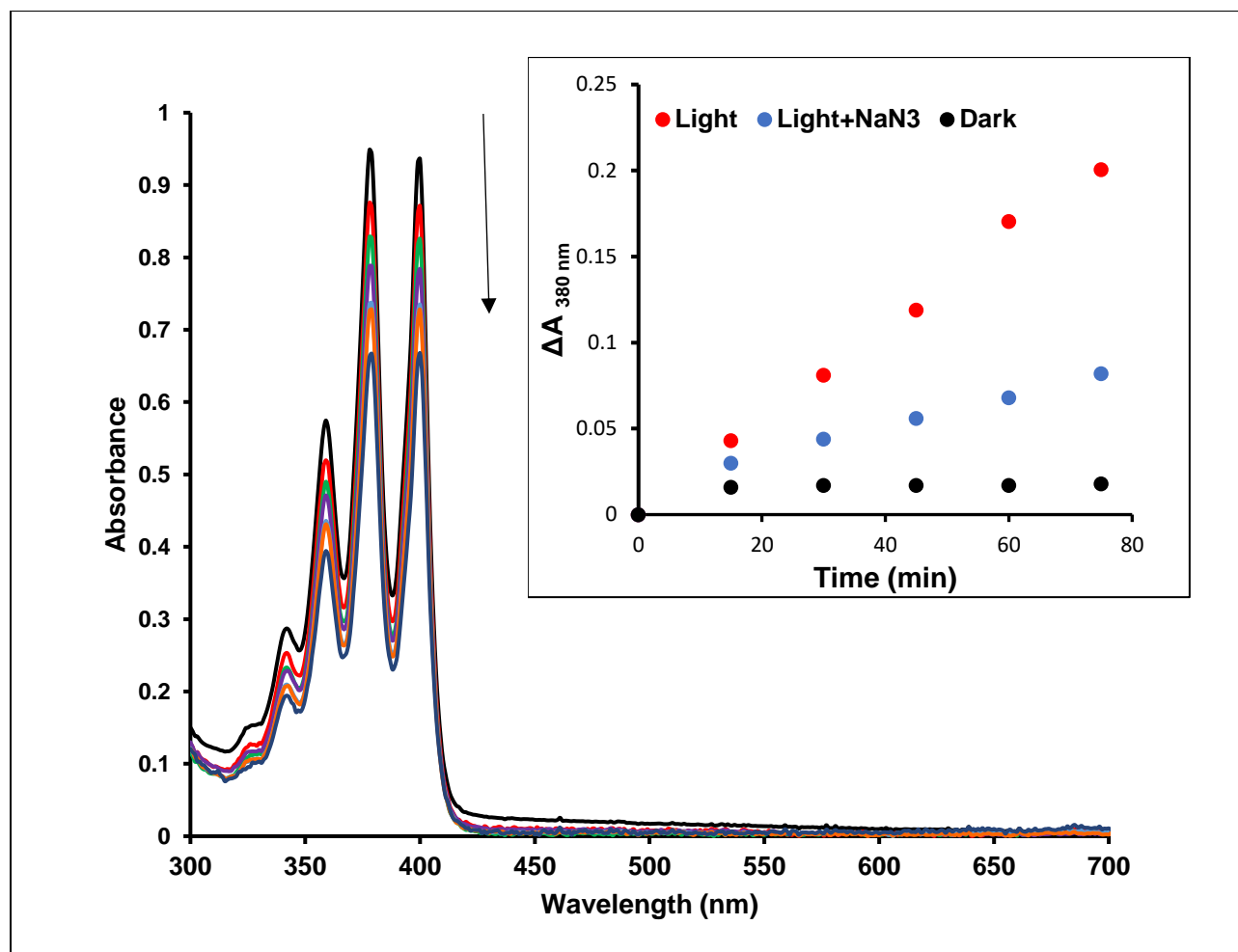


Figure 8: Absorption changes of ADMA in water vs. time using GW-ZnMCPpC under irradiation with Modulight laser, irradiance = 450 mW/cm² (ADMA concentration = 4.5 × 10⁻⁵ M). **Insert: Plot of ΔA for ADMA (380 nm) when irradiated with light, in the presence of NaN₃, and in the dark.**

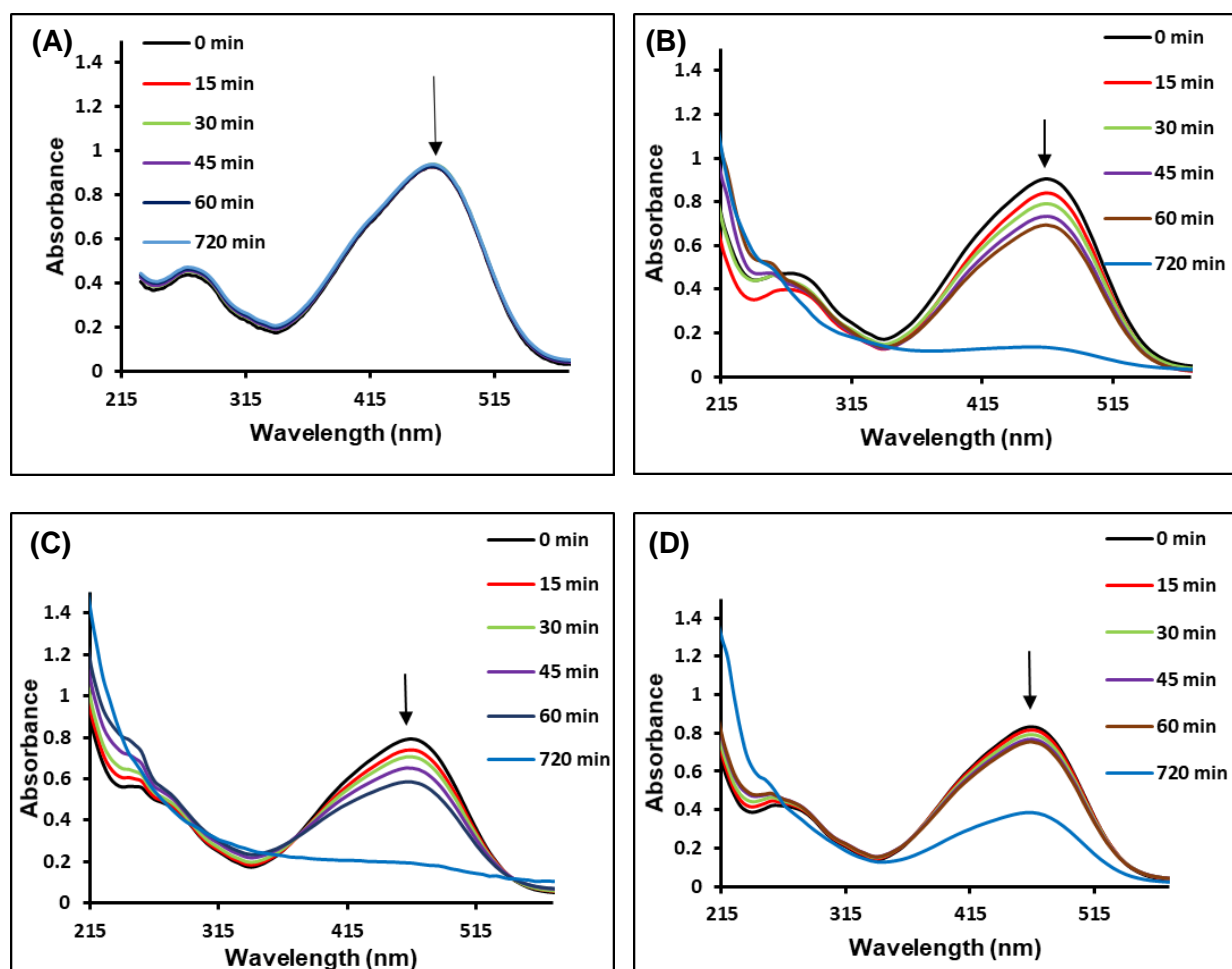


Figure 9: Time-dependent UV/Vis absorption analysis of photodegradation of methyl orange (3.3×10^{-5} M) in the presence of (A) GW, (B) GW-ZnMCPpC, (C) GW-ZnTCPPc, (D) GW-ZnMCPpC at pH 7.2, irradiance = 450 mW/cm².

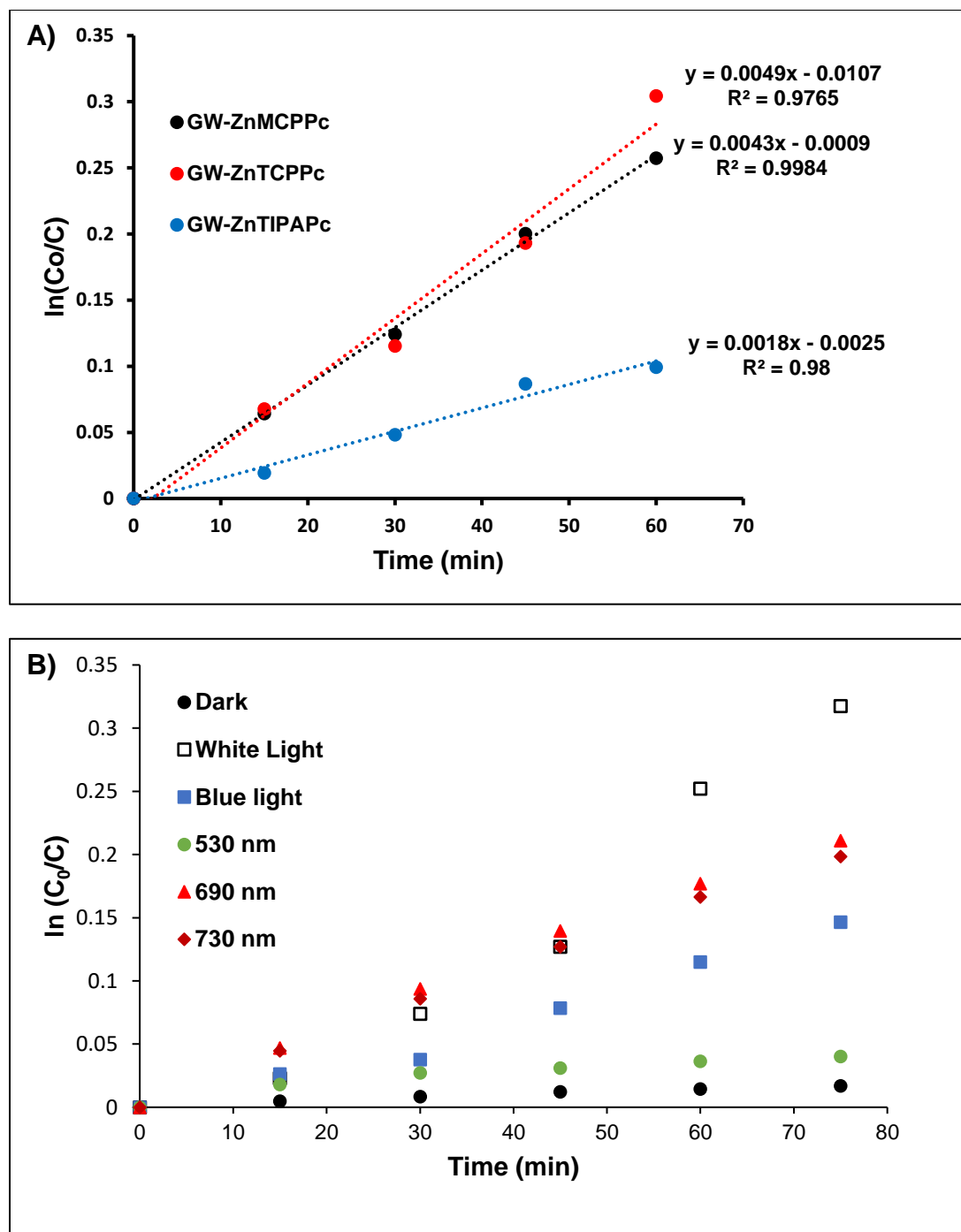


Figure 10: Time-dependent photodegradation of MO (3.3×10^{-5} M) upon A) irradiation with red light (Modulight-690 nm) in the presence of each Pc-GW composite and B) irradiation with varying light in the presence of GW-ZnMCPc.

Table 1: Q band maximum wavelength and singlet oxygen quantum yield values for ZnMCPc, ZnTCPPc, ZnTIPAPc, and Pc loading on GW.

Compound	Pc loading (wt% Pc on GW)	Q band λ (nm) ^a	Φ_{Δ} ^b	Φ_F
ZnMCPc	0.0365	674 (683)	0.40 (0.38)	0.16
ZnTCPPc	0.0334	678 (680)	0.44 (0.35)	0.09
ZnTIPAPc	0.0184	680 (686)	0.24 (0.22)	0.06

^aValues in brackets are for the GW- ZnPc conjugates in the solid-state and shows the monomer peak. ^bValues in brackets are for GW-ZnPc derivatives in aqueous media (5% DMSO).

Table 2: Photo-degradation of methyl orange using GW-ZnMCPc, GW-ZnTCPPc, and GW-ZnTIPAPc (cycle 1).

[MO]×10 ⁵ (mol/L)	<i>k</i> _{obs} (10 ⁻³ min ⁻¹)			Rate (10 ⁻⁷ mol L ⁻¹ min ⁻¹)			t _{1/2} (min)		
	GW-	GW-	GW-	GW-	GW-	GW-	GW-	GW-	GW-
	ZnMCPc	ZnTCPPc	ZnTIPAPc	ZnMCPc	ZnTCPPc	ZnTIPAPc	ZnMCPc	ZnTCPPc	ZnTIPAPc
1.65	8.1	7.8	5.0	1.34	1.29	0.83	86	89	139
3.30	4.9	4.3	1.8	1.62	1.42	0.59	141	161	385
4.95	3.8	3.4	0.9	1.88	1.68	0.45	182	204	770
6.60	3.2	2.5	0.4	2.11	1.65	0.26	217	277	1733
8.25	2.8	2.1	0.1	2.31	1.73	0.08	248	330	6931

Table 3: Comparison of GW-Pc conjugates with literature for the degradation of methyl orange

Catalyst	$k_{\text{obs}}/\text{min}^{-1}$ (% efficiency)	[MO] ($\times 10^{-5}$) M	Ref
(ZnMIPPC)-ZnO nanofibers	0.0099	2.80	43
FeTPP/TiO ₂ /CPVC	0.0049	50 m/L	44
3-TCbZnPc/PS	0.00253	2.31	45
ZnTCPC-Au@SiO ₂	0.0094	2.58	46
GW-ZnMCPPc	0.0049 (100%)	3.30	This work
GW-ZnTCPPc	0.0043 (93%)		This work
GW-ZnTIPAPc	0.0018 min ⁻¹ (44%)		This work

ZnMIPPC = (2-[5-(phenoxy)-isophthalic acid]-9(10),16(17),23(24)-tri-tert-butyl phthalocyaninato, TPP = tetraphenylporphyrin; CPVC = Chlorinated polyvinyl chloride.